Polymer 54 (2013) 812–818

Contents lists available at SciVerse ScienceDirect

Polymer

journal homepage: www.elsevier.com/locate/polymer

Investigation of CO_2 sorption in molten polymers at high pressures using Raman line imaging

Oliver Sven Knauer [a,b], Maria Giovanna Pastore Carbone [c], Andreas Braeuer [a,b,*], Ernesto Di Maio [c,**], Alfred Leipertz [a,b]

[a] Erlangen Graduate School in Advanced Optical Technologies (SAOT), Friedrich-Alexander-Universität Erlangen-Nürnberg, Paul-Gordan-Str. 6, 91052 Erlangen, Germany
[b] Lehrstuhl für Technische Thermodynamik (LTT), Friedrich-Alexander-Universität Erlangen-Nürnberg, Am Weichselgarten 8, 91058 Erlangen, Germany
[c] Department of Material and Production Engineering, Faculty of Engineering, University of Naples Federico II, Piazzale Tecchio 80, 80125 Naples, Italy

ARTICLE INFO

Article history:
Received 20 July 2012
Received in revised form
20 November 2012
Accepted 20 November 2012
Available online 29 November 2012

Keywords:
Diffusion
Solubility
Raman spectroscopy

ABSTRACT

CO_2 sorption in molten poly(ε-caprolactone) (PCL) has been investigated by temporally resolved Raman line imaging, which is introduced here as a new technology for the direct measurement of gas mass fraction profiles inside polymers during transient sorption experiments. Molten PCL was exposed to pressurized carbon dioxide in an optically accessible pressure cell at 80 °C and pressures up to 7.1 MPa. During sorption, Raman spectra were acquired temporally and spatially resolved across the PCL drop, allowing the evaluation of the PCL/CO_2 mutual diffusivity, of the CO_2 solubility in PCL, and the determination of temporal evolution of mass fraction profiles of carbon dioxide inside PCL.

1. Introduction

The production and processing of polymeric materials is generally assisted by the use of solvents, gases and additives, which are essential for optimizing production technologies and for achieving peculiar final structural/morphological properties. For instance, gas (e.g., carbon dioxide) application in the processing of polymers has gained tremendous ground especially in the fields of polymer foaming and recycling [1–4]. The main experimental techniques adopted for the quantitative measurement of the solubility and of the diffusivity of gases inside polymers are the pressure decay method [5], the gravimetric techniques [6], and the frequency modulation [7]. However, they are attended by several critical aspects [8,9]. Furthermore, those techniques provide an average measurement of the absorbed mass and not spatial information on gas concentration profiles evolving into the polymer, whose determination would give a more detailed frame of investigation on sorption as well as diffusion mechanisms in complex systems (for example, in polymer blends or in materials characterized by anomalous diffusion).

Information on the local concentration of gases in polymers can be obtained by spectroscopic techniques (ATR-FTIR and Raman), which have been extensively used for studying gas mass transport into polymers [10,11]. In particular, depth profiling by confocal Raman spectroscopy can be utilized for determining concentration profiles developing into the system under investigation. However, the Raman depth profile data are affected by the uncertainty of the z-position of the laser focus within the sample, due to optical aberrations to the focal volume [12]. Hence, several devices (both experimental and numerical) have been adopted for data correction [13].

Raman spectroscopy has been successfully applied for investigating heat and mass transfer [14], solubility [15], as well as diffusion [16] in different fields, e.g., the supercritical antisolvent process [17], hydrogen internal combustion engines [18], and carbon nanotubes generation [19]. In this work, we adopted a one-dimensional Raman set-up for the analysis of gas sorption in molten polymers. In particular, we have measured the temporal evolution of spatially-resolved CO_2 mass fraction profiles developing into a drop of molten poly(ε-caprolactone) (PCL) [20]. In comparison with the aforementioned spectroscopic techniques, such as Raman depth profiling, the advantage of this one-dimensional simultaneous acquisition of the gas mass fraction profile by Raman spectroscopy resides in the elimination of

* Corresponding author. Erlangen Graduate School in Advanced Optical Technologies (SAOT), Friedrich-Alexander-Universität Erlangen-Nürnberg, Paul-Gordan-Str. 6, 91052 Erlangen, Germany. Tel.: +49 9131 85 25853; fax: +49 9131 85 25851.
** Corresponding author. Tel.: +39 081 768 25 11; fax: +39 081 768 24 04.
E-mail addresses: Andreas.Braeuer@aot.uni-erlangen.de (A. Braeuer), edimaio@unina.it (E. Di Maio).

0032-3861/$ – see front matter © 2012 Elsevier Ltd. All rights reserved.
http://dx.doi.org/10.1016/j.polymer.2012.11.053

inaccuracies associated to the non-simultaneous acquisition of data, which is of particular importance when investigating rapidly evolving systems.

2. Theoretical background

The intensity of the detected Raman signal scattered from a molecule undergoing a transition from the energy level i before the scattering process to j after the scattering process, S_{ij}, is proportional to the molar concentration of scattering molecules n_{ij} and to a coefficient k_{ij} (based on literature [21])

$$S_{ij} \sim n_{ij}\left\{n_L\left(\frac{1}{\lambda_L}-\Delta\nu_{R,ij}\right)^4 L_{ij}\frac{\partial\sigma_{ij}}{\partial\Omega}\mathrm{d}\Omega\left[1-\exp\left(\frac{hc\Delta\nu_{R,ij}}{kT}\right)\right]^{-1} b_{ij}\right\} = n_{ij}k_{ij} \tag{1}$$

This coefficient comprises the influence of the number of excitation photons n_L, the wavelength of the laser excitation radiation λ_L, the Raman shift $\Delta\nu_{R,ij}$ of the transition, the strength of the local electromagnetic field L_{ij} (infuenced by the refractive index), the differential Raman scattering cross section σ_{ij}, the solid angle of the detection optics Ω, Planck's constant h, the speed of light c, the Boltzmann constant k, the temperature T, and an experimental constant b_{ij}, taking into account the efficiency of the optical components, the quantum efficiency of the detector and the efficiency of the spectrometer.

The ratio of the signals of two different Raman transitions, one from i to j and another one from k to l follows

$$\frac{S_{ij}}{S_{kl}} = \frac{n_{ij}}{n_{kl}}\frac{k_{ij}}{k_{kl}} = \frac{n_{ij}}{n_{kl}}K_{ij/kl}, \tag{2}$$

where $K_{ij/kl}$ is the ratio of k_{ij} to k_{kl}. Substituting the transitions ij and kl with a Raman transition of penetrant (p) and matrix (m), respectively, equation (2) reads

$$\frac{S_p}{S_m} = \frac{n_p}{n_m}K_{p/m}. \tag{3}$$

Hence, the ratio of the Raman signal intensities S_p and S_m is directly proportional to the ratio of the molar concentrations of penetrant, n_p, and of matrix, n_m. The combination of equations (1) and (3) provides the mole fraction of the penetrant (x_p) by

$$x_p = \frac{n_p}{n_p+n_m} = \frac{\frac{S_p}{k_p}}{\frac{S_p}{k_p}+\frac{S_m}{k_m}} = \frac{S_p}{S_p+S_m\frac{k_p}{k_m}} = \frac{1}{1+\frac{S_m}{S_p}K_{p/m}}, \tag{4}$$

or the mass fraction of the penetrant (w_p) by

$$w_p = \frac{m_p}{m_p+m_m} = \frac{\frac{S_pM_p}{k_p}}{\frac{S_pM_p}{k_p}+\frac{S_mM_m}{k_m}} = \frac{1}{1+\frac{S_mM_m}{S_pM_p}K_{p/m}}. \tag{5}$$

3. Experimental

3.1. Pendent polymer drop

Poly(ε-caprolactone), a biodegradable polymer with a melting point of ca. 60 °C, was supplied by Solvay Interox Ltd. (PCL CAPA 6800) and used as received. CO_2 with a purity of 99.5% was purchased by Linde, Germany.

Polymer drops were created by adopting titanium rods as drop holders. The rod was preliminarily fine polished to provide a very smooth and planar bottom surface, which is necessary for achieving drop radial symmetry. In order to avoid contamination with impurities, the rod was cleaned with acetone immediately before drop creation. The drop was then formed in an oven by melting a weighed amount of polymer on top of the polished surface of the rod, and then, turning around the system to avoid any polymer drainage. The oven was then cooled down to room temperature and, finally, the rod with the solid drop-like polymer adhering on it was mounted in the optically accessible measurement chamber.

The measurement chamber is a cubic stainless steel vessel of 90 mm edge length and approximately 120 mL inner volume. It is equipped with three round windows of 28 mm bore diameter. Two of the windows are arranged line in sight, to guide the laser beam through the vessel, and the third one is perpendicular to the others to detect the 90°-scattered light. A syringe pump fed pressurized CO_2 and a pressure sensor indicates the pressure in the vessel. The temperature of the chamber is controlled using four electric heating cartridges in the corners of the cubic vessel, a temperature controller and a Pt100 temperature sensor. Fig. 1 shows a typical hemispherical drop before and after CO_2 sorption. The green "line" indicates the position of the waist of the focus of the laser beam which passes directly through the center of the drop.

3.2. Optical setup

The excitation part of the Raman line imaging setup is shown in Fig. 2a. A frequency-doubled continuous wave laser Nd:YVO_4 laser with an output power of 3.5 W at a wavelength of 532 nm was used to excite the Raman signal inside the chamber. The combination of a plan concave lens (L1, $Ø = 1''$, $f = -10$ mm) and a plan convex lens (L2, $Ø = 2''$, $f = 1000$ mm) builds up a Galilean telescope and expands the circular shaped beam up to a diameter of approximately 45 mm. Another plane convex lens (L3, $Ø = 2''$, $f = 100$ mm) focuses the laser beam to the center of the chamber while a beam dump blocks the excitation laser light behind the chamber.

The setup to detect the Raman signals excited along the waist of the laser beam focus is shown in Fig. 2a in top and in Fig. 2b in side view. Along the waist of the laser beam focus, the laser power is concentrated in a small and approximately cylindrical volume resulting in a high excitation power and a high spatial resolution. The diameter of the focal beam waist can be assumed to be 100 μm. We used an achromatic lens with a small f-number (AC1, $Ø = 2''$, $f = 100$ mm) to detect the Raman signal through a large solid angle Ω. A long-pass filter ($Ø = 2''$, LP 532) blocks the elastically scattered light and transmits only the red-shifted Raman-Stokes signal. A

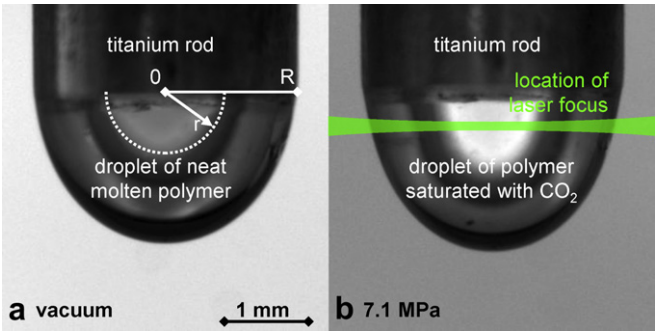

Fig. 1. Hemispherical PCL drop at 80 °C with a) definition of radial position and b) location of measurement volume.

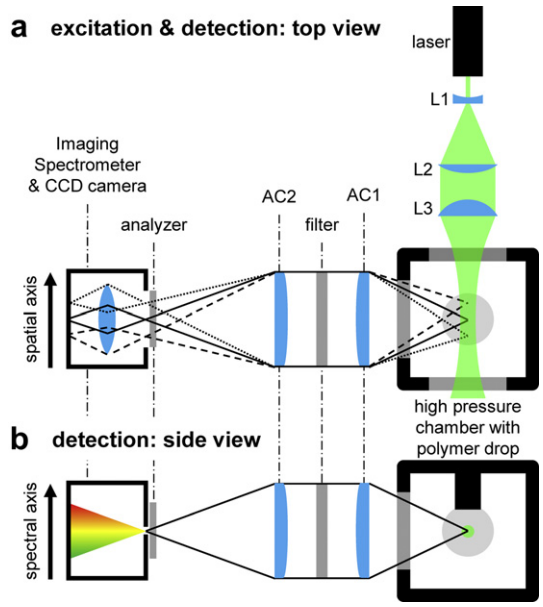

Fig. 2. Optical setup for a) excitation and detection in top view and b) detection in side view.

second achromatic lens (AC2, $\emptyset = 2''$, $f = 200$ mm) images the waist of the laser beam focus onto the entrance slit of an imaging spectrometer. As the imaging spectrometer conserves the spatial information along the waist of the laser beam focus (see top view in Fig. 2a), the Raman signal from different measurement positions is stored on neighboring pixels along the spatial axis of the CCD detector. The corresponding detector axis consists of 400 pixels of 16 μm border length each, so 6.4 mm in total length. Due to the magnification caused by the set of detection lenses (AC1 & AC2), the length of the measurement volume (waist of the laser beam focus) is 2.56 mm. As we binned 10 pixels along the spatial axis of the CCD detector, the length of the measurement volume of 2.56 mm could be resolved in 40 increments, each corresponding to 64 μm. The side view in Fig. 2b shows that the waist of the laser beam focus is imaged exactly on the 50 μm high entrance slit of the imaging spectrometer. The inelastically scattered light from each of the 40 measurement positions along the beam waist (measurement volume) is dispersed in its wavelength components along the spectral axis of the CCD detector. This 25.6 mm long chip axis consists of 1600 pixels of 16 μm border length each. With a ruled reflection grating of 1200 lines per mm optimized for 500 nm, a wavelength range of 546 nm up to 605 nm, corresponding to a Raman shift range of 480 cm^{-1} up to 2270 cm^{-1}, can be resolved. Summarizing, each image acquired with the camera behind the imaging spectrometer is composed of 40 Raman spectra, one for each of the 40 increments along the waist of the laser beam focus.

3.3. Testing procedure

Tests were performed at 80 °C and at carbon dioxide pressures up to 7.1 MPa. Before starting CO_2 pressurization the measuring chamber was evacuated (pressure was less than 1 kPa) by using a water jet pump in order to sort moisture out the polymer. Then, as the chamber was mounted on a three axes translation stage, the position of the drop was optimized with respect to the laser beam, as shown in Fig. 1b. In particular, the spectral information was acquired along a line from the center of the drop up to its surface. Because of drop radial symmetry, this geometrical configuration is sufficient for the investigation of diffusion phenomena.

A series of 50 back-to-back images (each one made up of 40 Raman spectra, acquired from the 40 increments along the 2.56 mm-long waist of the laser beam) was then acquired from pure PCL, with an exposure time of 6 s. Each pressure step was then started by opening a valve connecting the chamber with the pressurized syringe pump, providing the measurement pressure in less than 3 s. Immediately after the pressure step, images were recorded every 30 s, until the spectra did not show any variation in time, defining the attainment of equilibrium. For calibration purposes, series of 50 back-to-back images of the drop under CO_2 atmosphere at different pressures and in equilibrium were recorded likewise. All images were taken with the same camera settings at an exposure time of 6 s.

4. Results and discussion

4.1. Analysis of PCL/CO_2 spectra

Fig. 3 shows the equilibrium spectrum of pure PCL, acquired under vacuum. The Raman spectrum of pure PCL exhibits a typical fingerprint in the region between 500 and 1000 cm^{-1} and a series of peaks between 1033 and 1107 cm^{-1}, which have been assigned to the skeletal stretching. However, the strongest peaks can be found at 1295 cm^{-1} (assigned to ωCH_2), at 1430 cm^{-1} (to δCH_2), and at 1722 cm^{-1} (to $\nu C=O$) [22]. The spectra of the CO_2 saturated PCL after the attainment of the equilibrium are labeled by the corresponding pressure values in Fig. 3, clearly revealing the increasing contribution of the gas with increasing pressure. In fact, the upper Fermi dyad of CO_2 at 1372 cm^{-1}, whose intensity increases with CO_2 pressure, can be clearly identified in the spectra. The lower Fermi dyad at 1265 cm^{-1} can be found in the spectra of the solution too, but as it is superimposed with the ωCH2 peak of PCL, it can hardly be recognized in the spectra at the lowest gas pressure (1.9 MPa). It is interesting noticing that the positions of the Fermi dyads are shifted towards lower wavenumbers compared to gaseous CO_2, where they are located at 1388 cm^{-1} and 1285 cm^{-1} [23], respectively. This effect has been already observed when CO_2 is

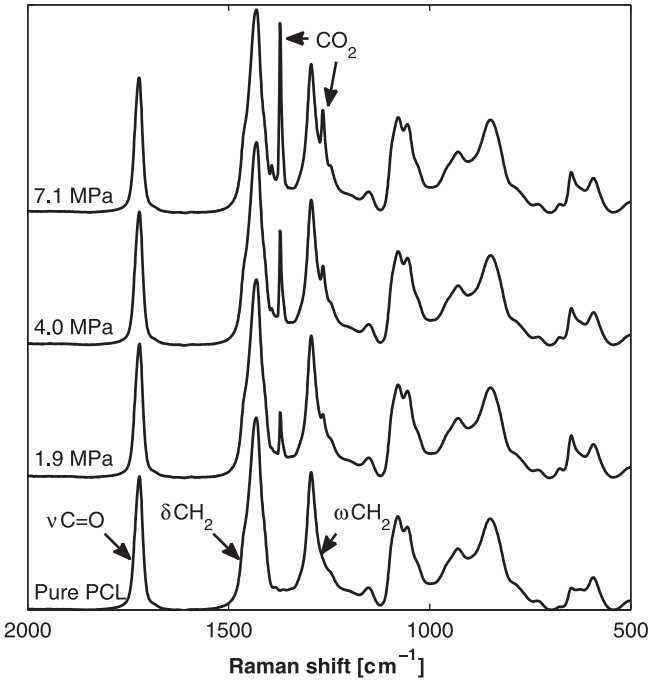

Fig. 3. Equilibrium Raman spectra of PCL and PCL-CO_2 solutions at 80 °C.

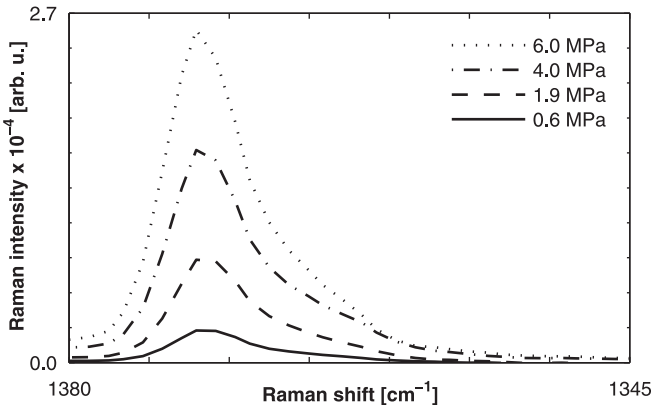

Fig. 4. Upper Fermi dyad of CO_2 obtained from difference spectra of solutions and pure polymer.

interacting with other polymers as PMMA [16] or clathrate hydrates [24].

The experimental set-up allows the acquisition of spatially and temporally resolved Raman spectra. In order to receive information on the temporal evolution of CO_2 mass fraction at each radial position, raw spectra have been treated as follows:

1. The series of 50 back-to-back images acquired from pure PCL were averaged and, for each spatial position, the mean Raman spectrum was background corrected by subtracting a spline and normalized to the integrated intensity of the peak between 1612 cm^{-1} and 1825 cm^{-1}, which has been assigned to the νC = O stretching of PCL.
2. The same spline subtraction and normalization procedure was carried out for each image of the PCL/CO_2 solution series acquired during transient sorption experiment and at equilibrium.
3. In order to isolate the CO_2 contribution in the solution, for each spatial position, the normalized Raman spectrum of the pure polymer was subtracted from the normalized Raman spectrum of the PCL/CO_2 solution. Due to identical background subtraction and normalization strategies, only the Fermi dyads of CO_2 remain in the difference spectra. As the lower Fermi dyad of CO_2 superimposes with the ωCH_2 peak of PCL, only the upper Fermi dyad is used here to calculate the CO_2 contribution, and the Raman signal of CO_2, S_{CO_2}, can be calculated as the integrated signal intensity in the wavenumber range from 1346 cm^{-1} up to 1380 cm^{-1}.

Fig. 4 shows the resulting Raman spectra at equilibrium for selected pressures within the limited wavelength range selected for calculating the contribution of CO_2 (S_{CO_2}). It is evident that S_{CO_2} increases with increasing pressure. In particular, as highlighted by equation (1), the higher intensity of the Fermi dyads in solution spectra is indicative of a higher concentration of CO_2 in the polymer.

Through the acquisition of spatially and temporally resolved Raman spectra, the proposed technique allows the detailed investigation of gas sorption mechanism. As an example, Fig. 5a shows

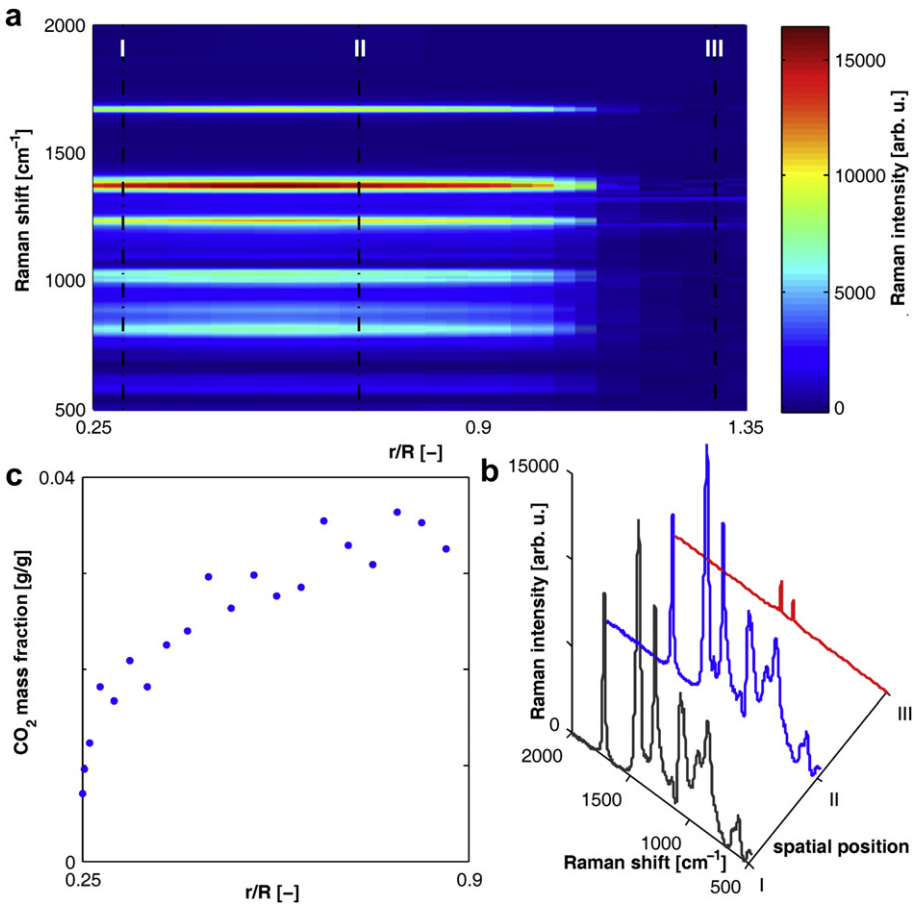

Fig. 5. a) Image acquired at t = 180 s. b) Raman spectra at selected radial positions. c) mass fraction profile derived according to equation (8).

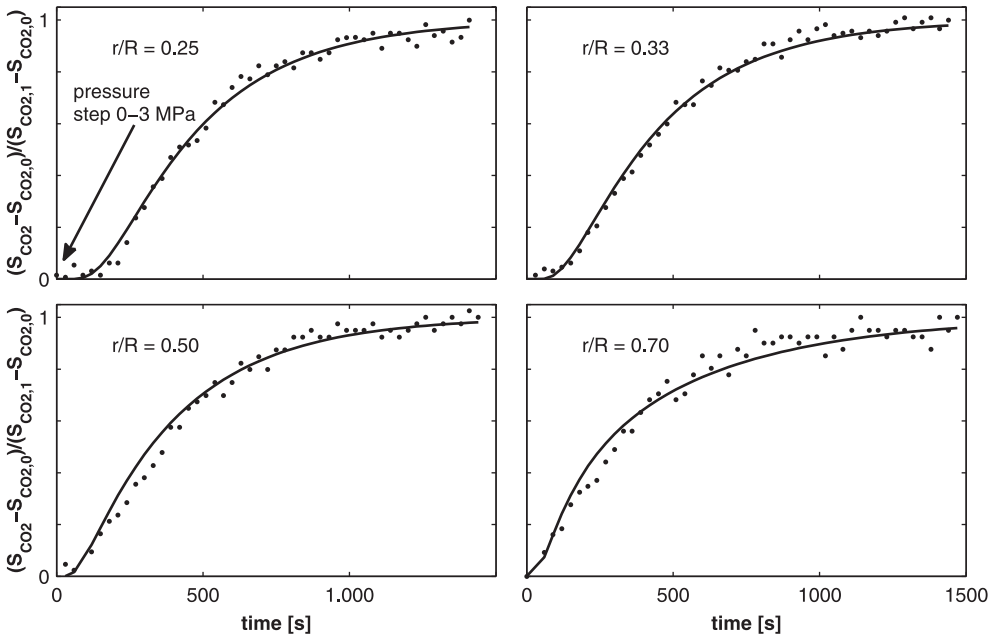

Fig. 6. Normalized integrated Raman signal intensity as a function of time at selected radial positions inside the drop for a pressure increase from 0 to 3.0 MPa at 80 °C. The experimental data (●) are fitted (—) to equation (7).

an image acquired at $t = 180$ s after the pressure step from 0 to 3.0 MPa. The spatial (horizontal axis) describes the position inside the measurement volume, converted to values of normalized radius (see Fig. 1a). The spectral axis gives the Raman shift, while the corresponding Raman signal is indicated by the color map. At three exemplary locations, indicated by Roman numerals (I – III), the corresponding spectra are plotted in Fig. 5b. Inside the drop, up to values of $r/R = 1$, the Raman spectra are characteristic for CO_2 dissolved in PCL, indicating a higher amount of CO_2 closer to the surface of the drop (II) than near the center (I). Outside the drop ($r/R > 1$), the Fermi dyads of pure CO_2 can be identified (III). By analyzing the spectrum of each spatial position, a mass fraction profile of CO_2 in the polymer drop can be derived (see Fig. 5c), as described in the section *Mass fraction profile*. As the drop center is not accessible (see Fig. 1), the resulting profile starts from a normalized radius value of 0.25 and range up to $r/R = 0.9$. Due to optical distortions caused by the drop curvature, the obtained mass fraction values are not reliable closer to the surface.

Additionally to the temporally resolved mass fraction profiles, the PCL/CO_2 mutual diffusivity (D) and of the CO_2 solubility in PCL can be derived from the Raman measurements. The corresponding evaluation strategies are reported in detail in the following sections.

4.2. Evaluation of the PCL/CO_2 mutual diffusivity

Assuming the bottom half of the drop to be a hemisphere and a Fickian diffusion behavior [25] for the PCL/CO_2 system at the experimental conditions, spatial and temporal evolution of the molar concentration of CO_2, n is described by the following expression [26].

$$\frac{n-n_o}{n_1-n_o} = 1+\frac{2R}{\pi r}\sum_{k=1}^{\infty}\frac{(-1)^k}{k}\sin\frac{k\pi r}{R}\exp\left(-Dk^2\pi^2 t/R^2\right). \qquad (6)$$

here, t is the time, r is the radial coordinate, R is the radius of the hemisphere, n_o is the initial concentration of CO_2 in the system and n_1 is the surface concentration (at $r = R$ and for $t \geq 0$). Due to the normalization strategy described above and according to equation (1), the calculated Raman signal of CO_2, S_{CO_2} is directly proportional to the ratio of molar concentrations n_{CO_2}/n_{PCL}. A constant PCL molar concentration n_{PCL} is assumed, as the maximum volume expansion during sorption is below 5% for pressures up to 3 MPa [8]. Hence, S_{CO_2} can be used instead of CO_2 concentration in equation (6), and the diffusivity can be calculated from

$$\frac{S_{CO_2}-S_{CO_2,0}}{S_{CO_2,1}-S_{CO_2,0}} = 1+\frac{2R}{\pi r}\sum_{k=1}^{\infty}\frac{(-1)^k}{k}\sin\frac{k\pi r}{R}\exp\left(-Dk^2\pi^2 t/R^2\right), \qquad (7)$$

where $S_{CO_2,0}$ and $S_{CO_2,1}$ are the initial and the equilibrium Raman signals of CO_2, as evaluated according to the procedure described previously. Fig. 6 compares experimental and theoretical results at four exemplary spatial positions, for the immediate pressure step from 0 to 3.0 MPa. By fitting the data in the whole r and t range to

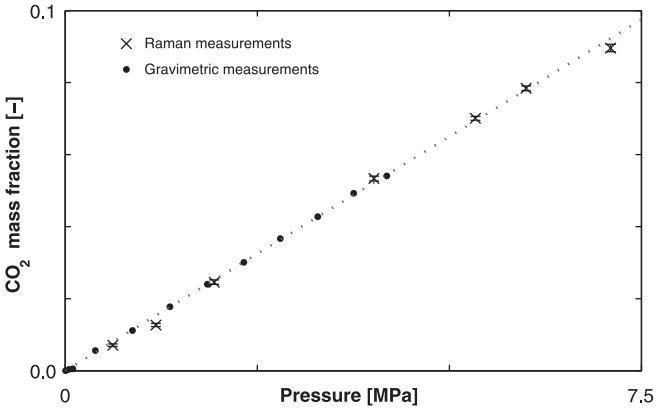

Fig. 7. Mass fraction calibration line. The error bars indicate the standard deviation of 20 measurement locations inside the drop.

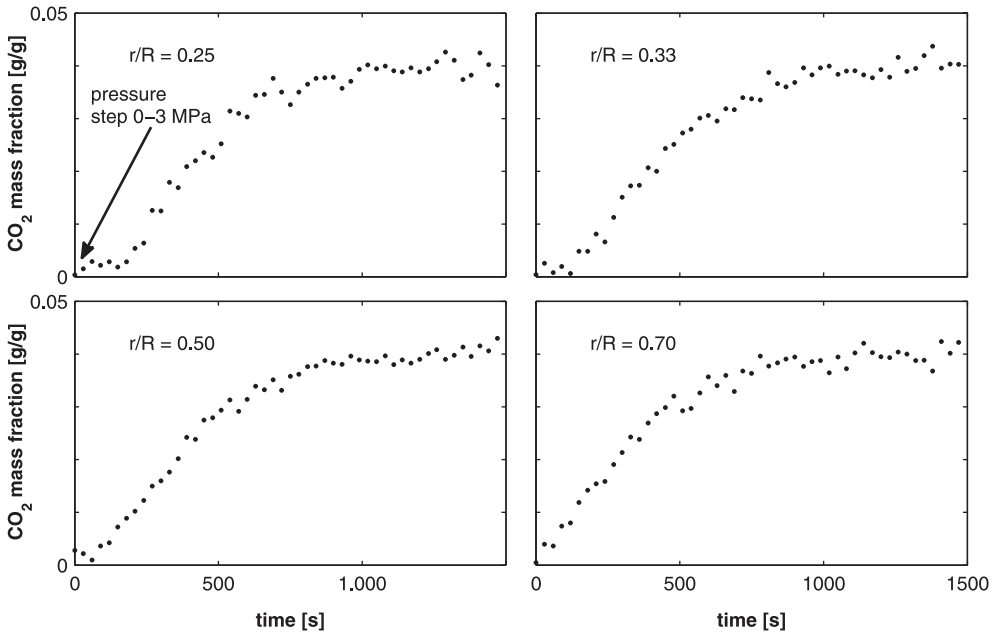

Fig. 8. Temporal evolution of CO_2 mass fraction at exemplary positions of the PCL drop. Data evaluated after the pressure increase from 0 to 3.0 MPa at 80 °C.

equation (7), D has been found equal to 7.1 ± 0.910^{-6} cm^2/s. This result is in accordance with gravimetric technique results, proving the reliability of the present approach [8,9]. It is worth of note, that the proposed procedure for the evaluation of D makes use of data on S_{CO_2} profiles evolution, due to the fact that CO_2 concentration is linearly related to S_{CO_2} and with the hypothesis of Fickian behavior of the investigated PCL/CO_2 system at specific testing conditions, without further assumptions (e.g. no S_{CO_2} vs. C calibration curve needed, as in the following evaluation of solubility). In principle, with this approach it is possible to measure diffusivities as high as 10^{-4} cm^2/s which is, however, the upper bound for gas diffusion in polymers. Nevertheless, pushing experimental conditions to the limit of the apparatus (Raman spectrum acquisition frequency as high as 10 s^{-1} and rod radius as large as the length of the measurement volume of 2.56 mm) may compromise the accuracy of the measurement as the former may worsen the quality of the Raman spectra and the latter may determine drop instability and/or would require large interfacial tension values to hold the drop.

4.3. Evaluation of the CO_2 solubility in PCL

Equation (5) correlates the Raman spectral information to mass fraction. As all the spectra have been normalized to the PCL Raman peak between 1612 cm^{-1} and 1825 cm^{-1}, the Raman signal intensity of PCL, S_{PCL}, can be assumed to be constant and unity, and simplifies equation (5) to:

$$\frac{m_{CO_2}}{m_{CO_2}+m_{PCL}} = \frac{1}{1+\dfrac{S_{PCL}M_{PCL}}{S_{CO_2}M_{CO_2}}K_{CO_2/PCL}} = \frac{S_{CO_2}}{S_{CO_2}+K'_{CO_2/PCL}}, \qquad (8)$$

where K'_{PCL/CO_2} takes into account the ratio of the molar masses M_{CO_2} to M_{PCL}. In order to calculate K'_{PCL/CO_2}, the equilibrium values of S_{CO_2} have been fitted to sorption data obtained for the same system by gravimetric experiments [8,9]. Fig. 7 reports the solubility data from literature [8,9], limited to 4.2 MPa, and the results of this calibration procedure, giving K'_{PCL/CO_2} equal to 2.3×10^{-6} with a coefficient of determination of $R^2 = 0.991$ and a root mean square error of RMSE $= 1.8 \times 10^{-3}$. This procedure allowed for the extension of the sorption isotherm up to 7.1 MPa, revealing a rather linear behavior up to high pressures. It is important to underline that, compared to the gravimetric measurements, the proposed approach provides reliable solubility data, as it does not suffer from any correction of the buoyancy effect due to any changes in specific volume of the polymer solution [8], that is commonly predominant at high pressures experiments.

4.4. Mass fraction profile

Having the calibration curve, the proposed measurement and elaboration strategy enables the quantitative, temporally and spatially resolved determination of CO_2 dissolved in PCL drops.

The temporal evolution of the spectral characteristic S_{CO_2} (as reported – normalized – in Fig. 6) has been converted, for each spatial position, into CO_2 mass fraction. Fig. 8 shows the temporal increase of the mass fraction of CO_2 dissolved in PCL for a pressure step from vacuum up to 3.0 MPa at several radial positions. For each measurement location, CO_2 mass fraction increases with time until a plateau is reached, indicating that the polymer drop has been saturated with CO_2 (attainment of the equilibrium). However, in the first 10 min, a different behavior is observed at the analyzed locations. At inner locations (r/R = 0.25, 0.33, 0.5), sorption kinetics exhibits a sigmoidal shape, characterized by an initial delay time. This characteristic time clearly increases as the measurement position approaches the center of the drop. The CO_2 diffusive path becomes longer for the inner zones of the drop and, consequently, a longer time is required until first detection of the penetrant can be observed.

5. Conclusions

Temporally resolved Raman line imaging was introduced to evaluate the composition of a pendent drop of molten PCL, exposed to pressurized carbon dioxide, at 80 °C and at pressures up to 7.1 MPa. PCL/CO_2 mutual diffusivity, CO_2 solubility in PCL and CO_2 mass fraction profiles have been evaluated in the investigated pressure range at a temperature of 80 °C. The spectra acquired from the PCL/CO_2 solution clearly revealed the contribution of the gas, as

the upper and the lower Fermi dyads of CO_2 could be clearly identified in the spectra. Furthermore, the intensity of the dyads increased with CO_2 pressure, revealing an increasing solubility in the polymer. Thus, information on gas mass fraction profiles evolving in the molten PCL could be straightforwardly derived from the spectra. The value of D has been found in accordance with gravimetric technique results, proving the reliability of the present approach. The sorption isotherm has been evaluated without any buoyancy correction, which could have affected the reliability of the results. Nevertheless, at normalized locations r/R smaller than 0.9, the computed mass fractions are in agreement with conventional sorption measurements. Due to these advantages, the Raman line imaging technique is recommended to be used for studying CO_2 mass transport and sorption thermodynamics in materials, which get in contact with CO_2 at elevated pressures. This might be interesting for the field of selective absorption of gases in advanced liquids, other foaming applications in general, and high pressure antisolvent technology. The most important prerequisite for the successful application of Raman line imaging investigations into the sorption of gases into liquids or solids is that the system under investigation has to be transparent for the wavelengths of the excitation laser and the Raman signals. As the Raman process can be excited with any wavelength, excitation lasers available on the market should be identifiable as those not absorbed by the substance. Unfortunately the attenuation and deflection of the excitation laser beam from interfaces is not significantly affected by the wavelength of the laser. Therefore, materials which look turbid – such as crystalline substances or materials with impurities or inclusions – will not allow the excitation laser beam to pass through the material making the acquisition of line profiles impossible.

Acknowledgments

The authors gratefully acknowledge the German Research Foundation (Deutsche Forschungsgemeinschaft – DFG) for funding the Erlangen Graduate School in Advanced Optical Technologies (SAOT) within the framework of the German Excellence Initiative.

References

[1] Kiran E. J Supercrit Fluids 2010;54(3):308–19.
[2] Kiran E. J Supercrit Fluids 2010;54(3):296–307.
[3] Kiran E. J Supercrit Fluids 2012;66(0):372–9.
[4] Tomasko DL, Li H, Liu D, Han X, Wingert MJ, Lee LJ, et al. Ind Eng Chem Res 2003;42(25):6431–56.
[5] Koros WJ, Paul DR. J Polym Sci B Polym Phys 1976;14(10):1903–7.
[6] Berens AR, Huvard GS. Interaction of polymers with near-critical carbon dioxide. In: Supercritical fluid science and technology, vol. 406. American Chemical Society; 1989. p. 207–23.
[7] Buttry DA, Ward MD. Chem Rev 1992;92(6):1355–79.
[8] Pastore Carbone MG, Di Maio E, Iannace S, Mensitieri G. Polym Test 2011; 30(3):303–9.
[9] Pastore Carbone MG, Di Maio E, Scherillo G, Mensitieri G, Iannace S. J Supercrit Fluids 2012;67(0):131–8.
[10] Takahashi M, Yamamoto Y, Nawaby AV, Handa YP. J Polym Sci B Polym Phys 2003;41(18):2214–7.
[11] Elabd YA, Baschetti MG, Barbari TA. J Polym Sci B Polym Phys 2003;41(22): 2794–807.
[12] Everall NJ. Appl Spectrosc 2000;54(10):1515–20.
[13] Tomba JP, Pastor JM. Macromol Chem Phys 2009;210(7):549–54.
[14] Knauer OS, Lang MC, Braeuer A, Leipertz A. J Raman Spectrosc 2011;42(2): 195–200.
[15] Rodriguez-Meizoso I, Lazor P, Turner C. J Supercrit Fluids 2012;65(0):87–92.
[16] Yoon J-H, Kawamura T, Takeya S, Jin S, Yamamoto Y, Komai T, et al. Macromolecules 2004;37(25):9302–4.
[17] Rossmann M, Braeuer A, Dowy S, Gallinger TG, Leipertz A, Schluecker E. J Supercrit Fluids 2012;66(0):350–8.
[18] Braeuer A, Engel SR, Hankel RF, Leipertz A. Opt Lett 2009;34(20):3122–4.
[19] Reinhold-López K, Braeuer A, Popovska N, Leipertz A. Opt Express 2010; 18(17):18223–8.
[20] Albertsson A-C, Varma I. Aliphatic polyesters: synthesis, properties and applications. In: Albertsson A-C, editor. Advances in polymer science, vol. 157. Berlin/Heidelberg: Springer; 2002. p. 1–40.
[21] Dowy S, Braeuer A, Schatz R, Schluecker E, Leipertz A. J Supercrit Fluids 2009; 48(3):195–202.
[22] Kister G, Cassanas G, Bergounhon M, Hoarau D, Vert M. Polymer 2000;41(3): 925–32.
[23] Rosso KM, Bodnar RJ. Geochim Cosmochim Acta 1995;59(19):3961–75.
[24] Sum AK, Burruss RC, Sloan ED. J Phys Chem B 1997;101(38):7371–7.
[25] Fick A. Ann Phys 1855;170(1):59–86.
[26] Crank J. Diffusion in a sphere. The mathematics of diffusion. Clarendon Press; 1979. p. 89–103.